Archives of Biochemistry and Biophysics 479 (2008) 52–62

Contents lists available at ScienceDirect

Archives of Biochemistry and Biophysics

journal homepage: www.elsevier.com/locate/yabbi

Structural basis of the differential binding of the SH3 domains of Grb2 adaptor to the guanine nucleotide exchange factor Sos1

Caleb B. McDonald, Kenneth L. Seldeen, Brian J. Deegan, Amjad Farooq *

Department of Biochemistry & Molecular Biology and the UM/Sylvester Braman Family Breast Cancer Institute, Leonard Miller School of Medicine, University of Miami, Miami, FL 33136, United States

ARTICLE INFO

Article history:
Received 13 June 2008
and in revised form 4 August 2008
Available online 26 August 2008

Keywords:
Grb2 adaptor
SH3 domain
Guanine nucleotide exchange factor Sos1
Isothermal titration calorimetry
Protein–ligand thermodynamics

ABSTRACT

Grb2–Sos1 interaction, mediated by the canonical binding of N-terminal SH3 (nSH3) and C-terminal SH3 (cSH3) domains of Grb2 to a proline-rich sequence in Sos1, provides a key regulatory switch that relays signaling from activated receptor tyrosine kinases to downstream effector molecules such as Ras. Here, using isothermal titration calorimetry in combination with site-directed mutagenesis, we show that the nSH3 domain binds to a Sos1-derived peptide containing the proline-rich consensus motif PPVPPR with an affinity that is nearly threefold greater than that observed for the binding of cSH3 domain. We further demonstrate that such differential binding of nSH3 domain relative to the cSH3 domain is largely due to the requirement of a specific acidic residue in the RT loop of the β-barrel fold to engage in the formation of a salt bridge with the arginine residue in the consensus motif PPVPPR. While this role is fulfilled by an optimally positioned D15 in the nSH3 domain, the chemically distinct and structurally non-equivalent E171 substitutes in the case of the cSH3 domain. Additionally, our data suggest that salt tightly modulates the binding of both SH3 domains to Sos1 in a thermodynamically distinct manner. Our data further reveal that, while binding of both SH3 domains to Sos1 is under enthalpic control, the nSH3 binding suffers from entropic penalty in contrast to entropic gain accompanying the binding of cSH3, implying that the two domains employ differential thermodynamic mechanisms for Sos1 recognition. Our new findings are rationalized in the context of 3D structural models of SH3 domains in complex with the Sos1 peptide. Taken together, our study provides structural basis of the differential binding of SH3 domains of Grb2 to Sos1 and a detailed thermodynamic profile of this key protein–protein interaction pertinent to cellular signaling and cancer.

Adaptor proteins play a central role in mediating cellular signaling within and across cells. Grb2[1] is one such adaptor that couples activated receptor tyrosine kinases (RTKs) to downstream effectors and regulators such as Ras [1–4]. The critical role of Grb2 in cellular signaling is exquisitely demonstrated through defects in mice embryos upon the disruption of *grb2* gene [5]. Grb2 is a modular protein comprised of a central SH2 domain flanked between an N-terminal SH3 (nSH3) domain and a C-terminal SH3 (cSH3) domain, giving it an overall modular architecture of nSH3-SH2-cSH3 [1]. Grb2 recognizes activated RTKs by virtue of its SH2 domain to bind to tyrosine-phosphorylated (pY) sequences in the context of the consensus motif pYXN located within the cytoplasmic tails of a diverse array of receptors, including EGF and PDGF receptors [6,7]. Alternatively, Grb2 can also indirectly dock onto activated RTKs through the binding of its SH2 domain to pY sequences within the adaptor protein p52Shc [8,9]. Upon the interaction of Grb2 to RTKs directly or indirectly, the SH3 domains of Grb2 present a placid opportunity for a wide variety of proteins, containing proline-rich sequences, to be recruited to the inner membrane surface and thus engage in downstream cellular signaling cascades [3,10–17]. Among them, the guanine nucleotide exchange factor Sos1 is by far the best characterized downstream partner of Grb2 [3,10]. Upon recruitment to the inner membrane surface, Sos1 catalyzes the GDP-GTP exchange within the membrane-bound GTPase Ras and thereby switches on a key signaling circuit that involves the activation of MAPK cascade central to cellular proliferation, survival and differentiation [18,19].

Several studies have shown that the requirement of both SH3 domains of Grb2 is de rigueur for full and sustained activation of Ras [3,4,9,10]. However, biophysical analysis of the binding of SH3 domains of Grb2 to a Sos1-derived peptide containing the pro-

* Corresponding author. Fax: +1 305 243 3955.
E-mail address: amjad@farooqlab.net (A. Farooq).

[1] *Abbreviations used:* CD, circular dichroism; EGF, epidermal growth factor; Grb2, growth factor receptor binder 2; ITC, isothermal titration calorimetry; MALDI-TOF, matrix-assisted LASER desorption/ionization-time of flight; MAPK, mitogen-activated protein kinase; NMR, nuclear magnetic resonance; PDGF, platelet-derived growth factor; RTK, receptor tyrosine kinase; SEC, size exclusion chromatography; SH2, Src homology 2; SH3, Src homology 3; Shc, Src homology containing; Sos1, son of sevenless 1.

0003-9861/$ - see front matter © 2008 Elsevier Inc. All rights reserved.
doi:10.1016/j.abb.2008.08.012

line-rich consensus motif PPVPPR suggests that the affinity of the nSH3 domain for Sos1 is several-fold greater than that observed for the cSH3 domain [20]. Structural analysis reveals that the nSH3 domain of Grb2 binds to a Sos1 peptide containing the consensus motif PPVPPR in a canonical fashion [21–24]. The nSH3 domain adopts a characteristic β-barrel fold comprised of a pair of nearly-orthogonal β-sheets with each β-sheet containing three anti-parallel β-strands. The incoming Sos1 peptide docks against a largely hydrophobic binding cleft located on one face of the β-barrel. Upon binding to this cleft in the nSH3 domain, the Sos1 peptide adopts the relatively open left-handed polyproline type II helical conformation. In comparison with the binding modes of proline-rich ligands to other SH3 domains, the residues in the Sos1 peptide that account for its specificity to the nSH3 domain of Grb2 appear to be V_{+2} and R_{+5} within the consensus motif PPVPPR, according to the nomenclature suggested by Schreiber and co-workers [25], with the first proline within this motif designated zero. Alanine substitution of V_{+2} and R_{+5} individually indeed reduces the affinity of the Sos1 peptide for the nSH3 domain by about 10–20-fold [22]. Due to lower binding affinity, structural analysis of cSH3 domain in complex with a Sos1 peptide has not hitherto been possible but NMR analysis suggests that Sos1 binds to the cSH3 domain in a manner akin to that observed for its interaction with the nSH3 domain [20].

To address the structural basis of the differential binding of SH3 domains of Grb2 to Sos1, we performed pair-wise amino acid sequence alignment of nSH3 and cSH3 domains (Fig. 1a). Given that V_{+2} and R_{+5} within the consensus motif PPVPPR account for the binding specificity of Sos1 to nSH3 domain [22], we reasoned that the residues within the nSH3 domain in close spatial contact with V_{+2} and R_{+5} may hold the clue to unraveling the differential binding of nSH3 domain versus cSH3 domain to Sos1. Structural analysis of nSH3 domain in complex with a Sos1 peptide containing the consensus motif PPVPPR has previously indicated that V_{+2} inserts into a deep hydrophobic pocket formed by residues F9, W36 and Y52 within the nSH3 domain, while R_{+5} very likely engages in the formation of an energetically favorable salt bridge with acidic residues D15 and/or E16 located within the β1-β2 loop of the nSH3 domain [21,22]. The β1-β2 loop is more widely known as the RT loop in the context of the β-barrel fold of SH3 domains due to the observation that the mutations of arginine and threonine residues within this loop of the SH3 domain of Src tyrosine kinase are important determinants of its transforming potential [26]. Analysis of the amino acid sequence alignment reveals that the triplet of F9/W36/Y52 in the nSH3 domain is absolutely conserved in the cSH3 domain with the structurally equivalent residues being F167/W193/Y209 (Fig. 1a). Thus, the differential binding of nSH3 and cSH3 domains to Sos1 could not be explained in terms of the requirement of specific residues within the SH3 domain for stabilizing V_{+2} within the consensus motif PPVPPR. In contrast, while E16 in the nSH3 domain is absolutely conserved by the structurally equivalent E174 in the cSH3 domain, the same is not true for D15 in the nSH3 domain, which is substituted by the structurally equivalent G173 in the cSH3 domain. Assuming that it is D15 and not E16 in the nSH3 domain that salt bridges with R_{+5} within the consensus motif PPVPPR, this scenario could easily explain the differential binding of nSH3 and cSH3 domains to Sos1 as the substitution of a glycine for an aspartate at a critical salt bridging position would likely result in the partial loss of binding affinity. Interestingly, our sequence analysis further suggests that there may be more to this story. Although the cSH3 domain lacks an acidic residue at the structurally equivalent position occupied by

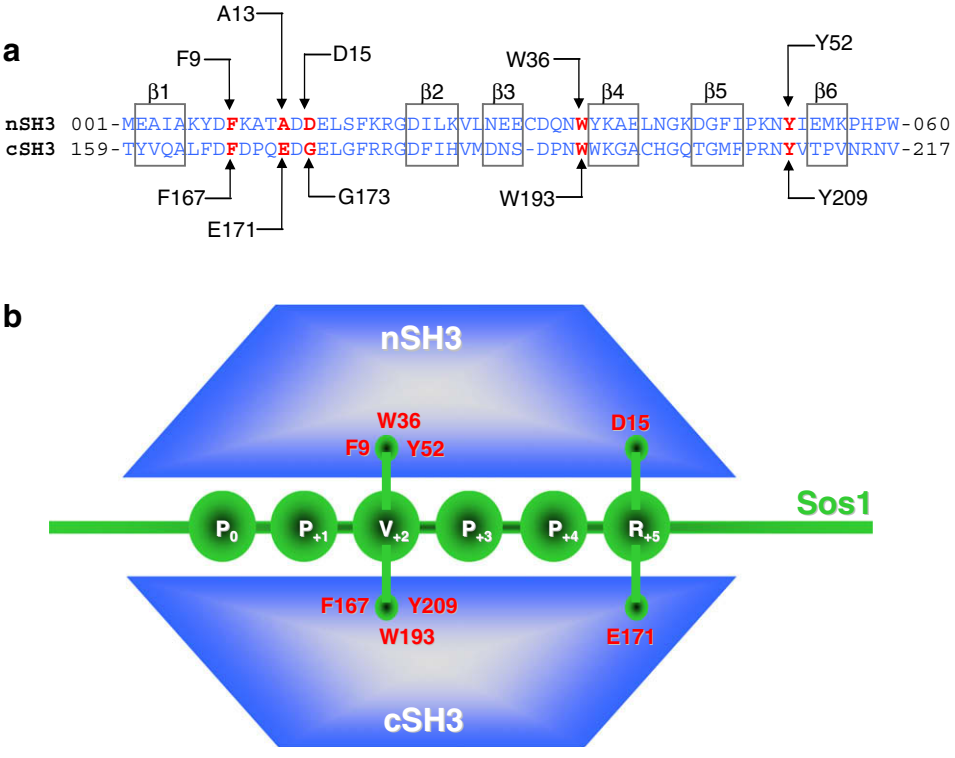

Fig. 1. Sequence analysis of SH3 domains of Grb2 and the proline-rich motif PPVPPR within the Sos1 peptide. (a) Sequence alignment of nSH3 and cSH3 domains of Grb2 highlighting the structurally equivalent residues. The residues in each of the six strands β1-β6, as observed in the 3D structure of the nSH3 domain [21–24], constituting the β-barrel fold are boxed. The residues in the SH3 domains predicted to be involved in stabilizing hydrophobic and electrostatic interactions, respectively due to the valine and the arginine in the Sos1 proline-rich motif PPVPPR are colored red. Note that the C32 in the β3-β4 loop of the nSH3 domain is deleted in the cSH3 domain. (b) A cartoon diagram showing the residues in the SH3 domains predicted to be involved in stabilizing hydrophobic and electrostatic interactions, respectively due to the valine and the arginine in the Sos1 proline-rich motif PPVPPR. (For interpretation of the references to color in this figure legend the reader is referred to the web version of the paper.)

D15 in the nSH3 domain, the residue E171 lies within close proximity to G173 within the RT loop and thus could be a strong candidate for fulfilling the role of a salt bridging partner for R_{+5} within the consensus motif PPVPPR. In light of the foregoing argument, we hypothesize that the differential binding of nSH3 and cSH3 domains to a Sos1 peptide containing the consensus motif PPVPPR is likely due to the ability of D15 within the nSH3 domain to salt bridge with R_{+5}, while this role may only partially be fulfilled by a chemically distinct and structurally non-equivalent residue E171 in the cSH3 domain due to the absence of an acidic residue at the structurally equivalent position D15 (Fig. 1b).

In an effort to test the above hypothesis, we have employed here isothermal titration calorimetry in combination with site-directed mutagenesis to determine complete thermodynamic signatures of the binding of various wildtype and mutant SH3 domains of Grb2 to a Sos1-derived peptide containing the consensus motif PPVPPR. Our data show that the nSH3 domain binds to a Sos1-derived peptide containing the proline-rich consensus motif PPVPPR with an affinity that is nearly threefold greater than that observed for the binding of cSH3 domain. We further demonstrate that such differential binding of nSH3 domain relative to the cSH3 domain is largely due to the requirement of a specific acidic residue in the RT loop of the β-barrel fold to engage in the formation of a salt bridge with the arginine residue in the consensus motif PPVPPR. While this role is fulfilled by an optimally positioned D15 in the nSH3 domain, the chemically distinct and structurally non-equivalent E171 substitutes in the case of the cSH3 domain. Additionally, our data suggest that salt tightly modulates the binding of both SH3 domains to Sos1 in a thermodynamically distinct manner. Our data further reveal that, while binding of both SH3 domains to Sos1 is under enthalpic control, the nSH3 binding suffers from entropic penalty in contrast to entropic gain accompanying the binding of cSH3, implying that the two domains employ differential thermodynamic mechanisms for Sos1 recognition. Our new findings are rationalized in the context of 3D structural models of SH3 domains in complex with the Sos1 peptide. Taken together, our study provides structural basis of the differential binding of SH3 domains of Grb2 to Sos1 and a detailed thermodynamic profile of this key protein–protein interaction pertinent to cellular signaling and cancer.

Materials and methods

Protein preparation

nSH3 (residues 1–56) and cSH3 (residues 156–217) domains of human Grb2 (Expasy# P62993) were cloned into pET102 bacterial expression vector – with an N-terminal thioredoxin (Trx)-tag followed by a thrombin site and a C-terminal polyhistidine (His)-tag preceded by a thrombin site – using Invitrogen TOPO technology. Trx-tag was included to maximize protein expression in soluble fraction, while the His-tag was added to aid in protein purification by Ni-NTA affinity chromatography. Additionally, thrombin protease sites were introduced at both the N- and C-termini of the protein to aid in the removal of tags after protein purification. The proteins were expressed in *Escherichia coli* Rosetta2(DE3) bacterial strain (Novagen) cultured in LB media and purified on Ni-NTA affinity column using standard procedures. Further treatment of the recombinant proteins on a MonoQ ion-exchange column and a Hiload Superdex 200 size-exclusion column coupled to GE Akta FPLC system led to purification of recombinant nSH3 and cSH3 domains to apparent homogeneity as judged by SDS-PAGE analysis. The identity of recombinant domains was further confirmed by MALDI-TOF mass spectrometry analysis. Protein yield was typically between 20 and 30 mg of recombinant domain of apparent homogeneity per liter of bacterial culture. The treatment of recombinant domains with thrombin protease significantly destabilized them and rendered them proteolytically unstable. For this reason, all experiments reported herein were carried out on recombinant fusion nSH3 and cSH3 domains containing a Trx-tag at the N-terminus and a His-tag at the C-terminus. The tags were found to have no effect on the functional properties of either domain. Protein concentrations were determined by both fluorescence using Invitrogen Quant-It assay and absorbance at 280 nm using an extinction co-efficient of 24,075 $M^{-1}\,cm^{-1}$ for the nSH3 domains and 28,085 $M^{-1}\,cm^{-1}$ for the cSH3 domains. The extinction co-efficients were calculated from amino acid sequence alone using the online software ProtParam at ExPasy Server [27]. Results from both methods were in an excellent agreement.

Site-directed mutagenesis

pET102 bacterial expression vectors expressing wildtype nSH3 (nSH3_WT) and wildtype cSH3 (cSH3_WT) domains of Grb2 were subjected to Stratagene Quickchange II site-directed mutagenesis to generate D15G (nSH3_D15G) and A13E (nSH3_A13E) mutants of the nSH3 domain and G173D (cSH3_G173D) and E171A (cSH3_E171A) mutants of the cSH3 domain. All mutant domains were expressed, purified and characterized as described above. When analyzed by size-exclusion chromatography (SEC) using Superdex 200 column, all mutant SH3 domains exhibited virtually indistinguishable elution volumes to those observed for the wildtype SH3 domains, implying that the point substitution of specific residues did not lead to protein unfolding and that the mutant SH3 domains retained the compact globular fold characteristic of wildtype SH3 domains. These observations were further confirmed by circular dichroism (CD) analysis.

Peptide synthesis

HPLC-grade 12-residue peptide PVPPPVPPRRRP spanning residues 1148–1159 within human Sos1 protein (Expasy# Q07889) and corresponding to the binding site for the SH3 domains of Grb2 was commercially obtained from GenScript Corporation. The peptide concentration was measured gravimetrically.

ITC measurements

Isothermal titration calorimetry (ITC) experiments were performed on Microcal VP-ITC instrument and data were acquired and processed using fully automized features in Microcal ORIGIN software. All measurements were repeated three to four times. Briefly, SH3 domain samples were prepared in Tris buffer (50 mM Tris, 200 mM NaCl, 1 mM EDTA and 5 mM β-mercaptoethanol at pH 8.0) or phosphate buffer (50 mM sodium phosphate, 200 mM NaCl, 1 mM EDTA and 5 mM β-mercaptoethanol at pH 8.0) or 50 mM Tris, 1 mM EDTA and 5 mM β-mercaptoethanol containing 0–300 mM NaCl at pH 8.0 and de-gassed using the ThermoVac accessory for 5 min. The experiments were initiated by injecting 25 × 10 μl injections of 1–4 mM of Sos1 peptide from the syringe into the calorimetric cell containing 1.8 ml of 50–200 μM of an SH3 domain solution at 25 °C. The change in thermal power as a function of each injection was automatically recorded using Microcal ORIGIN software and the raw data were further processed to yield binding isotherms of heat release per injection as a function of peptide to protein molar ratio. The heats of mixing and dilution were subtracted from the heat of binding per injection by carrying out a control experiment in which the same buffer in the calorimetric cell was titrated against the Sos1 peptide in an identical manner. Control experiments with scrambled peptides generated similar thermal power to that obtained

for the buffer alone – as did the titration of Sos1 peptide against a protein construct containing thioredoxin with a C-terminal His-tag (Trx-His). Titration of concentrated Trx-His protein construct into the calorimetric cell containing an SH3 domain solution produced no observable signal, implying that neither Trx-tag nor His-tag interact with any of the wildtype or mutant SH3 domains. To extract binding affinity (K_d) and binding enthalpy (ΔH), the binding isotherms were iteratively fit to the following built-in function by non-linear least squares regression analysis using the integrated Microcal ORIGIN software:

$$q(i) = (n\Delta HVP/2)\{[1 + (L/nP) + (K_d/nP)] - [[1 + (L/nP) + (K_d/nP)]^2 - (4L/nP)]^{1/2}\} \quad (1)$$

where $q(i)$ is the heat release (kcal/mol) for the ith injection, n is the binding stoichiometry, V is the effective volume of protein solution in the calorimetric cell (1.46 ml), P is the total protein concentration in the calorimetric cell (μM) and L is the total concentration of peptide ligand added (μM). The above equation is derived from the binding of a ligand to a macromolecule using the law of mass action assuming a 1:1 binding stoichiometry [28]. The free energy change (ΔG) upon ligand binding was calculated from the relationship:

$$\Delta G = RT \ln K_d \quad (2)$$

where R is the universal molar gas constant (1.99 cal/K/mol), T is the absolute temperature in Kelvins and K_d is in the units of mol/L. The entropic contribution ($T\Delta S$) to the free energy of binding was calculated from the relationship:

$$T\Delta S = \Delta H - \Delta G \quad (3)$$

where ΔH and ΔG are as defined above. The free energy change (ΔG) upon ligand binding can be dissected into two major constituent components by the following relationship:

$$\Delta G = \Delta G_{lig} + \Delta G_{ion} \quad (4)$$

where ΔG_{lig} is the contribution due to direct ligand binding and ΔG_{ion} is the contribution due to the indirect displacement of counterions upon ligand binding. ΔG_{ion} at a given NaCl concentration was calculated from the following relationship based on polyelectrolyte theory [29–32]:

$$\Delta G_{ion} = \psi RT \ln[NaCl] \quad (5)$$

where ψ is the fractional degree of net counterions displaced upon ligand binding. ψ was calculated from the slope of a plot of $\ln K_d$ versus ln[NaCl] assuming the following linear relationship based on thermodynamic linkage [29–32]:

$$\ln K_d = \psi \ln[NaCl] \quad (6)$$

With the knowledge of ΔG and ΔG_{ion}, Eq. (4) was re-arranged to obtain ΔG_{lig}.

Structural analysis

3D structures of SH3 domains of Grb2 in complex with the Sos1 peptide were modeled using the MODELLER software based on homology modeling [33]. In each case, the NMR structure of Grb2 nSH3 domain in complex with a Sos1-derived peptide containing the consensus motif PPVPPR (with a PDB code of 4GBQ) was used as a template. For the nSH3-Sos1 complex, hydrogen bonding restraints were added between the sidechain carboxylic oxygen atoms OD1 and OD2 of D15 in the nSH3 domain and sidechain guanidinium nitrogen atoms NH1 and NH2 of R_{+5} residue in the consensus motif PPVPPR. For the cSH3-Sos1 complex, hydrogen bonding restraints were added between the sidechain carboxylic oxygen atoms OE1 and OE2 of E171 in the cSH3 domain and sidechain guanidinium nitrogen atoms NH1 and NH2 of R_{+5} residue in the consensus motif PPVPPR. Hydrogen bonding restraints were necessary to bring the sidechains of respective residues within optimal hydrogen bonding distance in agreement with our thermodynamic data. In each case, a total of 100 structural models were calculated and the structure with the lowest energy, as judged by the MODELLER Objective Function, was selected for further energy minimization in MODELLER prior to analysis. The structures were rendered using RIBBONS [34] and electrostatic surface potential views were generated using MOLMOL [35]. All calculations were performed on the lowest energy structural model.

Results and discussion

Residues D15 and E171 underlie the differential binding of SH3 domains to Sos1

To test the differential binding of SH3 domains of Grb2 to Sos1, we expressed and purified the wildtype nSH3 (nSH3_WT) and the wildtype cSH3 (cSH3_WT) domains of Grb2 and measured their binding to the 12-residue Sos1 peptide PVPPPVPPRRRP containing the consensus motif PPVPPR using ITC. Additionally, we also generated various mutants of SH3 domains to map critical residues within both the nSH3 and cSH3 domains and measured their binding to the Sos1 peptide as described above. Because ligand binding can be coupled to other events such as protonation/deprotonation which can contribute to the magnitude of thermodynamic parameters with varying extents depending on the nature of the buffer, we performed our measurements in both Tris and phosphate buffers. Fig. 2 shows the representative ITC data for the binding of wildtype SH3 domains of Grb2 to the Sos1 peptide in Tris buffer. The binding affinities and the various thermodynamic parameters calculated from such data are presented in Table 1. The fact that various thermodynamic parameters are similar in both the Tris and phosphate buffers implies that the binding of SH3 domains to Sos1 peptide is not coupled to protonation/deprotonation events and that the thermodynamic parameters reported reflect actual values for the binding process.

As evidenced by our data in Table 1, the nSH3 domain binds to Sos1 with an affinity that is nearly threefold greater than that observed for the binding of cSH3 domain, implying that such differences arise from residues that are unique to each of the two SH3 domains. In order to determine the extent to which D15 in the nSH3 domain is critical as a salt bridging partner of R_{+5} in the consensus motif PPVPPR, the D15G mutant of nSH3 (nSH3_D15G) domain was generated. The rationale for the substitution of D15 to glycine instead of conventional alanine becomes obvious in light of the knowledge that G173 is the structurally equivalent residue in the cSH3 domain to D15 in the nSH3 domain (Fig. 1a). The fact that the D15G mutant reduces the binding of nSH3 domain to Sos1 by more than an order of magnitude suggests strongly that D15 plays the role of a salt bridging partner for R_{+5} and that the neighboring residues D14 and E16 cannot substitute for this role. In order to test the extent to which substitution of an aspartate for a glycine at position 173 in the cSH3 domain will restore its binding potential to a level similar to that observed for the nSH3 domain, the G173D mutant of cSH3 (cSH3_G173D) domain was generated. As expected, the G173D mutant augments the binding of the cSH3 domain to Sos1 to a level that is virtually indistinguishable from that of nSH3 domain. A corollary of our hypothesis is that E171 in the cSH3 domain may at least partially fulfill the role of D15 in the nSH3 domain. To test that this is so, we generated E171A mutant of cSH3 (cSH3_E171A) domain. The substitution of E171 to alanine may appear to be due to the relatively conservative and non-destructive properties of alanine but the logic for doing so here is of quite different nature. The residue that occupies struc-

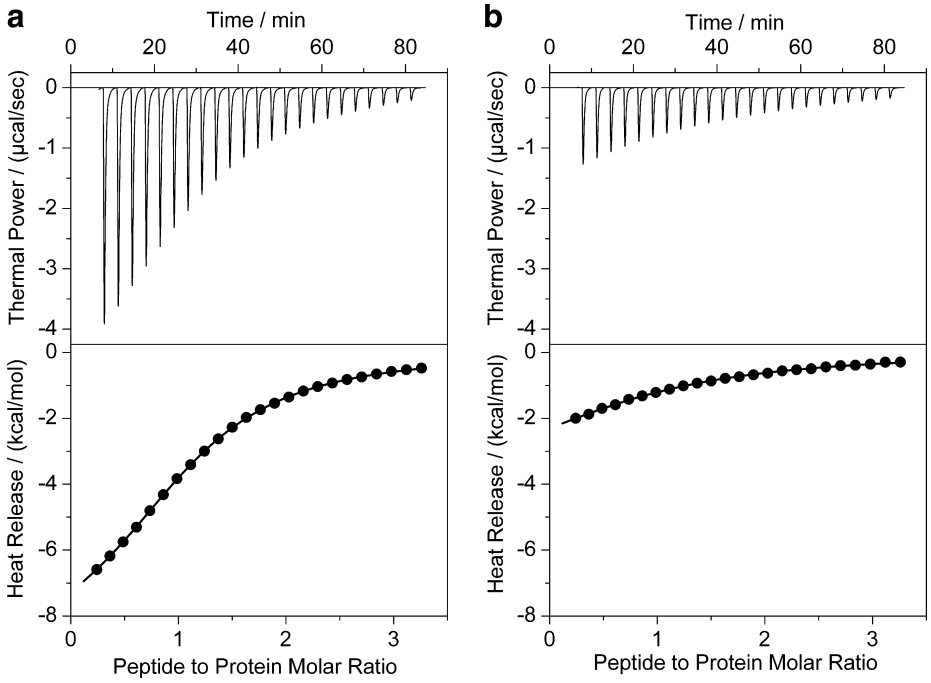

Fig. 2. ITC analysis of the binding of wildtype nSH3 (a) and wildtype cSH3 (b) domains of Grb2 to the Sos1 peptide PVPPPVPPRRRP in Tris buffer. For each data set, the corresponding SH3 domain in the calorimetric cell was titrated with 25 × 10 μl injections of the Sos1 peptide from the injection syringe at 25 °C. The first injection and the corresponding heat release are not shown due to systematic uncertainties in the measurement. The top panels show the raw ITC data describing the change in thermal power as a function of time upon subsequent injections. The raw data was processed to generate the binding isotherms of heat release per injection as a function of increasing Sos1 peptide to SH3 domain molar ratio as shown in the bottom panels. The solid lines represent the fit of the data in the binding isotherms to Eq. (1) based on the binding of a ligand to a macromolecule using the Microcal ORIGIN software [28]. All data are shown to the same scale for direct comparison.

Table 1
Experimentally determined thermodynamic parameters for the binding of various wildtype and mutant SH3 domains of Grb2 to the Sos1 peptide PVPPPVPPRRRP obtained from ITC measurements at 25 °C and pH 8.0 in Tris and phosphate buffers

	Tris				Phosphate			
	K_d (μM)	ΔH (kcal/mol)	$T\Delta S$ (kcal/mol)	ΔG (kcal/mol)	K_d (μM)	ΔH (kcal/mol)	$T\Delta S$ (kcal/mol)	ΔG (kcal/mol)
nSH3_WT	38.64 ± 2.38	−9.45 ± 0.01	−3.42 ± 0.03	−6.03 ± 0.04	49.89 ± 8.90	−9.28 ± 0.18	−3.40 ± 0.29	−5.87 ± 0.11
nSH3_D15G	459.78 ± 2.49	−14.53 ± 0.42	−9.97 ± 0.42	−4.56 ± 0.01	444.07 ± 75.58	−15.09 ± 0.03	−10.51 ± 0.13	−4.58 ± 0.10
nSH3_A13E	41.76 ± 0.86	−11.66 ± 0.08	−5.68 ± 0.09	−5.98 ± 0.01	40.99 ± 0.71	−11.69 ± 0.11	−5.70 ± 0.10	−5.99 ± 0.01
cSH3_WT	117.10 ± 1.82	−4.60 ± 0.05	+0.77 ± 0.06	−5.37 ± 0.01	120.19 ± 4.62	−4.81 ± 0.14	+0.54 ± 0.12	−5.35 ± 0.02
cSH3_E171A	847.52 ± 10.15	−12.89 ± 0.40	−8.69 ± 0.41	−4.20 ± 0.01	521.30 ± 41.95	−13.55 ± 0.49	−9.07 ± 0.54	−4.48 ± 0.05
cSH3_G173D	56.50 ± 0.49	−7.03 ± 0.14	−1.23 ± 0.13	−5.80 ± 0.01	64.02 ± 0.47	−6.99 ± 0.06	−1.21 ± 0.05	−5.73 ± 0.01

The values for K_d and ΔH were obtained from the fit of expression [1] based on the binding of a ligand to a macromolecule using the law of mass action assuming a 1:1 binding stoichiometry to ITC isotherms. The values for $T\Delta S$ were determined using Eq. (3). The values for ΔG were calculated using Eq. (2). The stoichiometries to the fits agreed to within ±10%. Errors were calculated from three to four independent measurements. All errors are given to one standard deviation.

turally equivalent position to E171 in the nSH3 domain is A13 and thus the mutant E171A bears the potential to play a double act in not only reporting the significance of the role of a glutamate but also that of alanine at this position (Fig. 1a). Consistent with our hypothesis, the E171A mutant reduces the binding of the cSH3 domain to Sos1 by nearly an order of magnitude, implying that this residue, at least in part, fulfills the role of D15 in the cSH3 domain in its ability to form a salt bridge with R_{+5}. This salient observation also suggests that the neighboring residues D172 and E174 in the cSH3 domain cannot substitute for the role of salt bridging with R_{+5}. Finally, to test whether a glutamate at position 13 may further augment the binding of nSH3 domain to Sos1, we generated the A13E mutant of nSH3 (nSH3_A13E) domain. The finding that the A13E mutant does not further augment the binding of nSH3 domain to Sos1 suggests that R_{+5} has either acquired a preference for salt bridging with a counterpart at position 15 over position 13, or alternatively, prefers an aspartate over a glutamate within the RT loop of the β-barrel fold.

In sum, our binding data discussed above unequivocally demonstrate that the higher affinity binding of nSH3 domain relative to cSH3 domain to Sos1 is largely attributable to the single residue D15 located within the RT loop of the β-barrel fold wherein it acts as a salt bridging partner for R_{+5}. Furthermore, the lack of an acidic residue at the structurally equivalent position of D15 in the cSH3 domain accounts for its lower binding affinity to Sos1 relative to the nSH3 domain. Nonetheless, this lower affinity binding of the cSH3 domain to Sos1 is dependent on E171 located within the RT loop of the β-barrel fold wherein it most likely engages in the formation of a salt bridge with R_{+5} in the consensus motif PPVPPR.

SH3 domains employ differential thermodynamic mechanisms for binding to Sos1

One of the unique features of ITC is that it provides a complete thermodynamic signature of two binding partners. As shown in Fig. 2 and Table 1, the binding of nSH3 and cSH3 domains of

Grb2 to Sos1 employs distinct thermodynamic mechanisms. While both interactions are driven by favorable enthalpic changes, the binding of nSH3 domain to Sos1 is accompanied by entropic penalty in contrast to entropic gain for the binding of cSH3 domain to Sos1.

What might be the molecular basis of these two opposing thermodynamic forces dictating the Grb2–Sos1 interaction? Release of heat usually results from the formation of bonds. It is thus conceivable that the formation of an extensive network of non-covalent interactions due to hydrophobic contacts, electrostatic interactions and hydrogen bonding between SH3 domains and Sos1 may account for the highly favorable enthalpic changes observed here. The formation of intermolecular hydrophobic contacts is most likely due to the bringing together of hydrophobic residues such as P_0, P_{+1}, V_{+2}, P_{+3} and P_{+4} in the consensus motif PPVPPR within the close vicinity of specific residues constituting the binding cleft of the β-barrel upon complexation as observed in the 3D structure of the nSH3 domain bound to a Sos1 peptide [21–24]. In contrast, the electrostatic interactions largely result from the formation of a salt bridge between R_{+5} in the consensus motif PPVPPR with D15 in the nSH3 domain or E171 in the cSH3 domain. Additional electrostatic interactions may be afforded by further salt bridging between arginine residues R_{+6} and R_{+7} in the Sos1 peptide and specific acidic residues in the SH3 domains [21,22]. However, these latter residues are likely to contribute little to the enthalpic gain observed due to the observation that their alanine substitution has little effect on the overall binding affinity of SH3 domains to Sos1 [22]. Finally, intermolecular hydrogen bonding between backbone carbonyl oxygens and amide hydrogens is also likely to contribute favorably to the enthalpic changes observed here. The overall entropic change accompanying molecular associations usually results from an inter-play between two major entropic players in the form of solvation entropy and conformational entropy [36–39]. The solvation entropy is due to the increase in the degrees of freedom of water molecules as a result of restructuring and displacement of water molecules from molecular surfaces, particularly from around the apolar groups, coming together. As such, the change in solvation entropy upon molecular associations contributes favorably to the overall entropic change. However, such favorable gain of entropy is largely offset and often overwhelmed by the unfavorable change in conformational entropy due to the loss in the degrees of freedom of backbone and sidechain atoms upon molecular associations. In light of the above-mentioned reasons, we attribute the entropic penalty observed for the binding of nSH3 domain to Sos1 largely to the loss in the degrees of freedom of backbone and sidechain atoms within both interacting partners, while the entropic gain observed for the binding of cSH3 domain to Sos1 is most likely due to the increase in the degrees of freedom of water molecules upon molecular association.

To gain further insights into the role of thermodynamic forces governing the binding of SH3 domains to Sos1, differential thermodynamic signatures for various pairs of wildtype and mutant SH3 domains are shown in Fig. 3. In this analysis, the magnitude and the sign of each of the three major differential thermodynamic parameters $\Delta\Delta H$, $T\Delta\Delta S$ and $\Delta\Delta G$ provide a graphical output of the differences in the underlying thermodynamic forces for the Sos1-binding of one SH3 domain relative to the other SH3 domain. While the magnitude of a given differential parameter, as judged by the height of the bar along the vertical axis, is indicative of its significance, the positive or negative sign of a given differential parameter dictates whether it is favorable or unfavorable depending on the type of thermodynamic force under consideration for the Sos1-binding of one SH3 domain relative to the other. Thus, a negative value of $\Delta\Delta H$ is indicative of enthalpy change being more favorable for the Sos1-binding of one SH3 domain relative to the other, while a positive value of $T\Delta\Delta S$ is indicative of entropy change being more favorable for

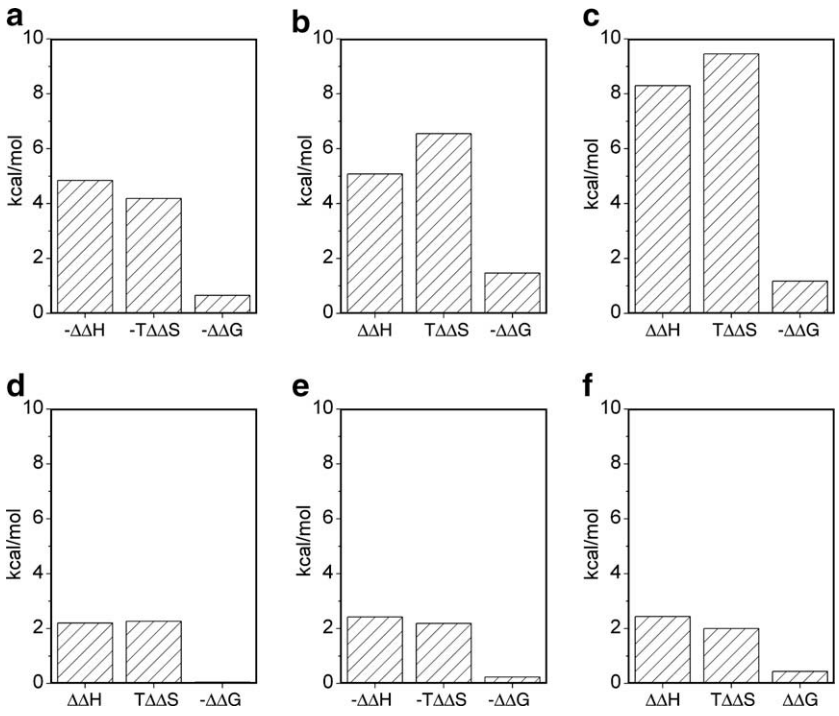

Fig. 3. Differential energetics for the binding of various wildtype and mutant SH3 domains of Grb2 to the Sos1 peptide PVPPPVPPRRRP in Tris buffer. Shown are the differential thermodynamic signatures for the Sos1-binding of one SH3 domain relative to the other SH3 domain: (a) nSH3_WT relative to cSH3_WT; (b) nSH3_WT relative to nSH3_D15G; (c) cSH3_WT relative to cSH3_E171A; (d) nSH3_WT relative to nSH3_A13E; (e) nSH3_WT relative to cSH3_G173D; and (f) cSH3_WT relative to cSH3_G173D. $\Delta\Delta H$, $T\Delta\Delta S$ and $\Delta\Delta G$ were calculated from the relationships $\Delta\Delta H = \Delta H_X - \Delta H_Y$, $T\Delta\Delta S = T\Delta S_X - T\Delta S_Y$ and $\Delta\Delta G = \Delta G_X - \Delta G_Y$, where the subscripts X and Y denote the corresponding thermodynamic parameters for the binding of one SH3 domain (SH3_X) and the other SH3 domain (SH3_Y) to the Sos1 peptide, respectively (Table 1). All plots are shown to the same scale for direct comparison.

the Sos1-binding of one SH3 domain relative to the other. As shown in Fig. 3a, it is evident that the Sos1-binding of nSH3_WT relative to cSH3_WT is enthalpically more favorable but entropically less favorable. Thus, the high affinity binding of nSH3_WT to Sos1 appears to be largely attributable to favorable enthalpic changes in lieu of favorable entropic changes. In striking contrast, the enthalpy change is less favorable while entropy change is more favorable for the Sos1-binding of nSH3_WT relative to nSH3_D15G despite diminished affinity of the latter by more than an order of magnitude (Fig. 3b). This salient observation implies that the formation of a salt bridge between R_{+5} in the consensus motif PPVPPR with D15 in the nSH3 domain is enthalpically unfavorable but entropically favorable, possibly due to the displacement of water molecules and the release of counterions from around the charged groups in R_{+5} and D15. That the formation of an intermolecular salt bridge may be accompanied by enthalpic penalty but entropic gain is further corroborated by the Sos1-binding of cSH3_WT relative to cSH3_E171A (Fig. 3c). In this latter scenario, the alanine substitution of E171, which appears to engage in the formation of a salt bridge with R_{+5} in the consensus motif PPVPPR, is concomitant with a substantial release of enthalpy despite the reduction in binding to Sos1 by nearly an order of magnitude. However, the favorable enthalpy change is more than offset by a large entropic penalty. The above-mentioned observations thus indicate that the role of salt bridge formation in the SH3–Sos1 interaction is to lower the overall entropic loss due to binding.

The structurally equivalent residue to E171 in the nSH3 domain is A13 but, while the binding affinities of Sos1-binding of nSH3_WT relative to nSH3_A13E are very similar (Table 1), the underlying energetics display some differences (Fig. 3d). On the same token, nSH3_WT binds to Sos1 with a similar affinity to that observed for cSH3_G173D but the two display different thermodynamic signatures (Fig. 3e). Interestingly, cSH3_G173D binds to Sos1 with an affinity that is over twofold greater than cSH3_WT but the differences in the underlying thermodynamic forces are no greater than those observed for the Sos1-binding of nSH3_WT relative to nSH3_A13E and for the Sos1-binding of nSH3_WT relative to cSH3_G173D (Fig. 3d–f). That this is so emphasizes the rather highly under-appreciated fact that similar binding affinities may not necessarily arise from similar underlying thermodynamic forces and vice versa. In particular, substitution of specific amino acids may alter the thermodynamics of molecular associations without having any effect on the overall binding affinities. Such thermodynamic differences may be attributable to the differences in the solvation properties of the sidechains of specific residues and their ability to engage in specific interactions. Thus, although the substitution G173D in the cSH3 domain enables it to bind to Sos1 with an affinity that is virtually same as that observed for the binding of nSH3 domain, analysis of underlying thermodynamic forces suggests that the differential binding of these two SH3 domains to Sos1 is not merely attributable to the presence of a glycine residue at position 173 instead of an aspartate but that other residues are also likely to play a role in determining specific protein–protein interactions. For example, it is possible that specific acidic residues within nSH3 and cSH3 domains may stabilize positive charge on R_{+6} and/or R_{+7} in the Sos1 peptide. Further mutagenesis studies are thus warranted to map the role of additional residues that may underlie the differential binding of nSH3 and cSH3 domains to Sos1. It should also be noted here that the above thermodynamic arguments are based on the assumption that the wildtype and mutant SH3 domains retain the same conformation. Although our SEC and CD analysis demonstrate that this is likely the case, the possibility that subtle conformational changes could occur between the wildtype and mutant domains cannot be excluded and thus such conformational changes could partially contribute to the differential thermodynamics observed here.

Salt tightly modulates the binding of SH3 domains to Sos1 in a thermodynamically distinct manner

Elucidating the extent to which the thermodynamics are dependent on ambient salt concentration can provide novel insights into protein–protein interactions. Given that electrostatic interactions appear to play a key role in the formation of Grb2–Sos1 complex, the dependence of thermodynamics of this important interaction on salt concentration thus cannot be overemphasized.

Fig. 4a shows the dependence of the equilibrium constant (K_d) for the binding of SH3 domains of Grb2 to the Sos1 peptide on NaCl concentration. It is evident from such data that the binding of both SH3 domains to Sos1 is highly sensitive to ambient salt concentration. Thus, while the K_d for the binding of nSH3 domain to Sos1 decreases by about fivefold from around 10 μM to over 50 μM over the NaCl concentration in the range of 0–300 mM, the K_d for the binding of cSH3 domain to Sos1 decreases by about threefold from around 50 μM to about 150 μM over the same NaCl concentration range. The K_d values of about 10 μM and 50 μM observed for the binding of nSH3 and cSH3 domains to Sos1 in the absence of NaCl are in good agreement with the values previously reported for this interaction in low salt buffers [20–22]. That salt modulates the binding of cSH3 domain to Sos1 to a much lesser degree relative to that observed for the binding of nSH3 domain suggests strongly that the release of counterions plays a much greater role in the formation of the latter complex. To quantitatively measure the extent to which counterion release governs the binding of SH3 domains of Grb2 to Sos1, we generated the salt linkage plots of $\ln K_d$ versus ln[NaCl] and calculated the fractional degree of net counterion release (ψ) from the corresponding slopes (Fig. 4a and Table 2). Our analysis shows that ψ is nearly twofold greater for the binding of nSH3 domain versus the cSH3 domain to Sos1, arguing in favor of a much greater role of counterion release in driving the nSH3–Sos1 interaction. It is believed that the release of counterions upon protein–ligand interactions is entropically favorable and thus contributes to the overall free energy of binding. As indicated in Table 2, the counterion release contributes to the overall free energy of binding to Sos1 by nearly twice as much for nSH3 domain relative to the cSH3 domain at NaCl concentration of 200 mM. In the absence of such favorable contributions, the binding of both SH3 domains to Sos1 would be expected to be lower by several folds.

That counterion release plays somewhat lesser role in dictating the Sos1-binding of cSH3 domain relative to nSH3 domain is further reflected in the salt-dependence of thermodynamic parameters ΔH and $T\Delta S$ (Fig. 4b). Thus, ΔH and $T\Delta S$ are highly sensitive to changes in salt for the binding of nSH3 domain to Sos1 and experience a change of nearly equal but opposing 10 kcal/mol in their contribution to ΔG over the NaCl concentration in the range of 0–300 mM. In contrast, ΔH and $T\Delta S$ exhibit poor dependence on salt for the binding of cSH3 domain to Sos1 and undergo a change of only about 1 kcal/mol in their contribution to ΔG over the same NaCl concentration. Despite such dramatic differences in the behavior of underlying ΔH and $T\Delta S$ on ambient salt concentration, ΔG appears to be tightly modulated in the binding of both SH3 domains to Sos1. That this is so further underlies the importance of thermodynamics to understanding protein–ligand interactions and emphasizes the fact that cellular processes may be modulated by salt through distinct thermodynamic mechanisms.

Thermodynamic data lead to structural refinement of SH3 domains bound to Sos1 peptide

In recent years, there has been growing interest in predicting the thermodynamics of protein–ligand interactions from structural information alone in what has come to be loosely defined as "structural thermodynamics" [39–42]. Whether structural thermo-

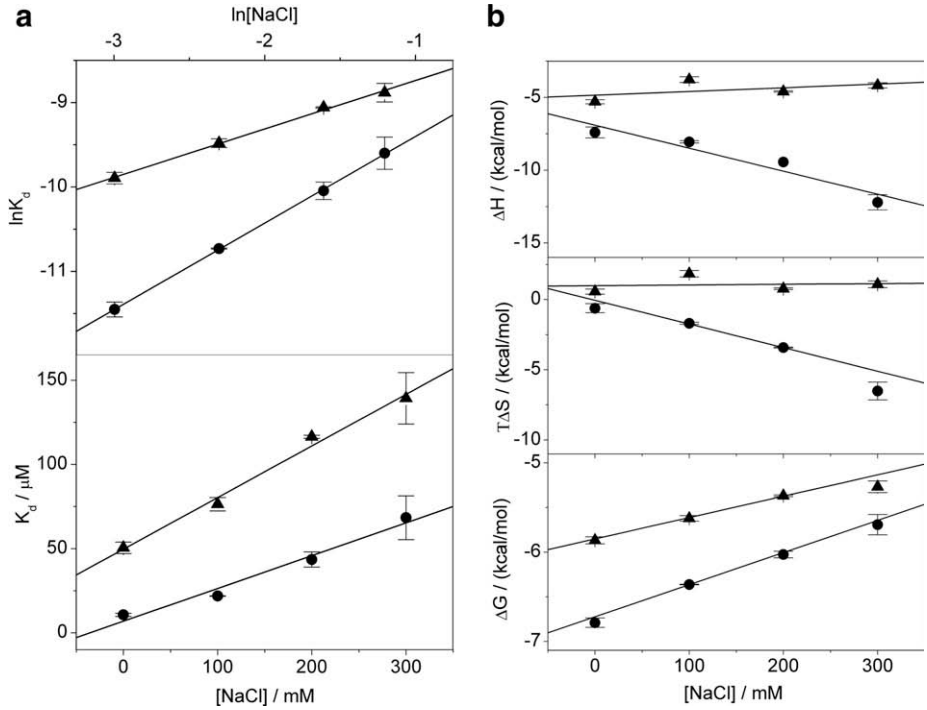

Fig. 4. Effect of salt on the binding of wildtype SH3 domains of Grb2 to the Sos1 peptide PVPPPVPPRRRP in 50 mM Tris, 1 mM EDTA and 5 mM β-mercaptoethanol containing 0–300 mM NaCl at pH 8.0. Each SH3 domain in the calorimetric cell was titrated with 25 × 10 μl injections of the Sos1 peptide from the injection syringe to obtain binding isotherms at NaCl concentrations in the range of 0–300 mM. To determine the various parameters, the binding isotherms at each NaCl concentration were fit to Eq. (1) based on the binding of a ligand to a macromolecule using the Microcal ORIGIN software. Each data point is the arithmetic mean of three to four experiments. All error bars are given to one standard deviation. (a) Dependence of K_d on NaCl concentration (lower panel) and the ln K_d versus ln[NaCl] plot (upper panel) used in the thermodynamic linkage analysis given by Eq. (6) for the binding of Sos1 peptide to nSH3 domain (●) and cSH3 domain (▲) of Grb2. [NaCl] and K_d in the upper panel were logarithmized in the standard units of mol/L. The solid lines show linear fits to the data points. (b) Dependence of thermodynamic parameters ΔH, $T\Delta S$ and ΔG on NaCl concentration for the binding of Sos1 peptide to nSH3 domain (●) and cSH3 domain (▲) of Grb2. The solid lines show linear fits to the data points.

Table 2
Experimentally determined thermodynamic parameters underlying the energetic contributions resulting from the counterion release upon the binding of wildtype SH3 domains of Grb2 to the Sos1 peptide PVPPPVPPRRRP obtained from ITC measurements at 25 °C and pH 8.0

	ψ	ΔG_{ion} (kcal/mol)	ΔG_{lig} (kcal/mol)	ΔG (kcal/mol)
nSH3_WT	1.03 ± 0.01	−0.98 ± 0.01	−5.05 ± 0.05	−6.03 ± 0.04
cSH3_WT	0.57 ± 0.01	−0.55 ± 0.01	−4.82 ± 0.01	−5.37 ± 0.01

The ψ values were obtained from the slopes of linear fits to ln K_d versus ln[NaCl] plots in 50 mM Tris, 1 mM EDTA and 5 mM β-mercaptoethanol containing 0–300 mM NaCl at pH 8.0 (Fig. 4a). The values for ΔG_{ion}, the free energy change due to counterion displacement, at 200 mM NaCl were determined using expression [5]. The values for ΔG_{lig}, the free energy change exclusively due to ligand binding, at 200 mM NaCl were calculated from Eq. (4). The values for ΔG, the overall free energy change for binding, at 200 mM NaCl were obtained from Eq. (2). Errors were calculated from three to four independent measurements. All errors are given to one standard deviation.

dynamics will deliver what it promises remains to be seen but few would doubt that the identification of key residues involved in protein–ligand interactions through a combination of thermodynamic analysis coupled with site-directed mutagenesis can often lead to refinement of structural data. Although the structures of nSH3 domain of Grb2 in complex with Sos1-derived peptides containing the consensus motif PPVPPR have been reported time and again [21–24], the role of many residues critical to this protein–ligand recognition remains to be ascertained. Thus, for example, it has hitherto not been known whether D15 or E16 fulfilled the role of salt bridging partner for R_{+5} within the consensus motif PPVPPR. Due to lower binding affinity, structural analysis of cSH3 domain in complex with a Sos1-derived peptide has not been possible to date but NMR analysis suggests that Sos1 binds to the cSH3 domain in a manner akin to that observed for its interaction with the nSH3 domain [20]. In an attempt to refine the nSH3–Sos1 structure and to determine de novo structure of the cSH3 domain bound to Sos1 consistent with our thermodynamic data reported here, we used homology modeling in combination with various hydrogen bonding distance restraints to calculate new 3D structures of these two complexes (Fig. 5).

As expected, the 3D structure of each SH3 domain in complex with the Sos1 peptide containing the consensus motif PPVPPR adopts a characteristic β-barrel fold comprised of a pair of nearly-orthogonal β-sheets with each β-sheet containing three anti-parallel β-strands (Fig. 5a and b). The strands β1-β2-β6 constitute the first β-sheet, while the second β-sheet is comprised of strands β3-β4-β5. The loop β1-β2 within the β-barrel is more widely referred to as the "RT loop" due to the observation that the mutations of arginine and threonine residues within this loop of the SH3 domain of Src tyrosine kinase are important determinants of its transforming potential [26]. It should be noted here that the curving of β-sheets around each other imparts on SH3 domains a more β-barrel-like shape in contrast to a β-sandwich in which the β-sheets tend to be straighter relative to each other. The incoming Sos1 peptide docks against a largely hydrophobic binding cleft located on one face of the β-barrel. Apart from the deep binding cleft, both SH3 domains adopt a near-spherical shape and appear to be somewhat electrostatically polarized – the negative charge is largely localized on the peptide binding face of each molecule with little or no negative charge on the opposite side (Fig. 5c and d).

Upon binding to the SH3 domain, the Sos1 peptide adopts the relatively open left-handed polyproline type II helical conformation. Within the binding cleft, there are two key sub-sites that

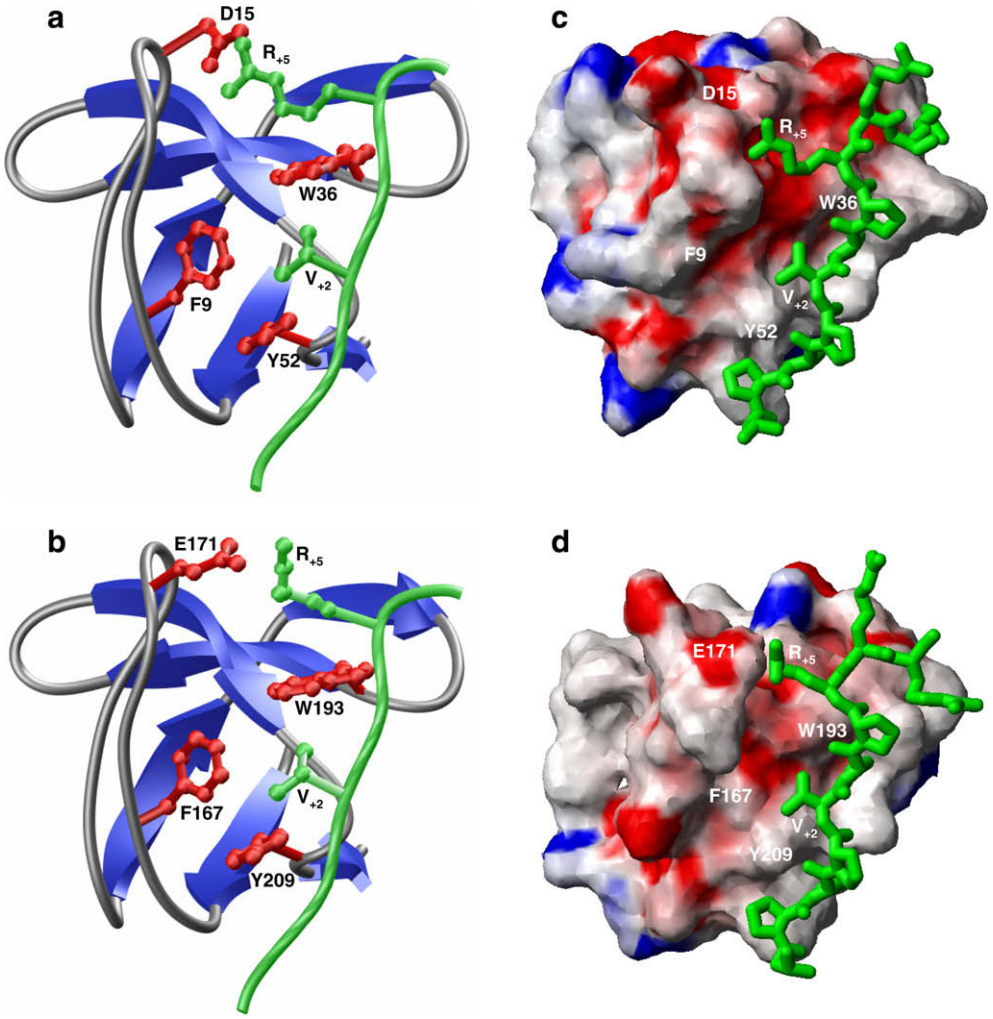

Fig. 5. 3D structures of wildtype SH3 domains of Grb2 in complex with the Sos1 peptide PVPPPVPPRRRP obtained from homology modeling and using hydrogen bonding restraints consistent with thermodynamic data reported here. (a) Ribbon representation of nSH3 domain bound to Sos1 peptide. The nSH3 domain is shown in blue with loops depicted in gray and the sidechains of residues that stabilize the V_{+2} and R_{+5} residues in the Sos1 peptide are colored red. The Sos1 peptide, including the sidechains of V_{+2} and R_{+5} residues, is colored green. (b) Ribbon representation of cSH3 domain bound to Sos1 peptide. The cSH3 domain is shown in blue with loops depicted in gray and the sidechains of residues that stabilize the V_{+2} and R_{+5} residues in the Sos1 peptide are colored red. The Sos1 peptide, including the sidechains of V_{+2} and R_{+5} residues, is colored green. (c) Electrostatic surface potential view of nSH3 domain. The blue and red colors respectively denote the density of positive and negative charges, while the hydrophobic and neutral surfaces are indicated by white/gray color. The Sos1 peptide, including the sidechain of all residues, is shown in green. (d) Electrostatic surface potential view of cSH3 domain. The blue and red colors respectively denote the density of positive and negative charges, while the hydrophobic and neutral surfaces are indicated by white/gray color. The Sos1 peptide, including the sidechain of all residues, is shown in green. (For interpretation of the references to color in this figure legend the reader is referred to the web version of the paper.)

account for the binding specificity of SH3 domains of Grb2 to Sos1. Firstly, the triplet of residues constituted by F9/Y52/W36 in the nSH3 domain and F167/Y209/W193 in the cSH3 domain forms a "cradle" that exquisitely accommodates the V_{+2} residue in the consensus motif PPVPPR. While the alanine substitution of V_{+2} decreases the affinity of Sos1 peptide for the nSH3 domain by nearly an order of magnitude [22], the relative contribution of F9/F167, Y52/Y209 and W36/W193 to the binding energy has not been analyzed to date. While the tight modulation of SH3–Sos1 interaction by changes in ambient salt concentrations as observed here is unlikely to be accounted for by the cradeling of V_{+2}, the stabilization of Sos1 peptide at a second sub-site via the formation of a salt bridge offers no better suspect. Here, the formation of ion pairs between D15 in the nSH3 domain and E171 in the cSH3 domain with the R_{+5} residue in the consensus motif PPVPPR generates much needed entropic contribution to the binding energy due to the release of counterions as supported by our thermodynamic data (Table 2). Destabilization of these ion pairs reduces the binding affinity to Sos1 by nearly an order of magnitude in the case of cSH3 domain, while its impact on nSH3 domain is even more pronounced (Table 1). It would be fitting to add here that the differential binding of nSH3 and cSH3 domains to Sos1 seems to be largely due to differences in the chemistry of the ion pair formation with the R_{+5} residue in the consensus motif PPVPPR. While this role is fulfilled by D15 in the nSH3 domain, the structurally equivalent residue in the cSH3 domain is G173. As a consequence of this, the cSH3 domain relies on the neighboring E171 to step up and although the role of E171 in neutralizing the charge on R_{+5} residue cannot be disputed, this interaction seems to be far from optimal and results in substantial reduction in the binding affinity of cSH3 domain relative to nSH3 domain. This view is supported by the fact that the G173D mutant of cSH3 domain binds to Sos1 with an affinity that is virtually indistinguishable from the binding of nSH3 domain (Table 1).

Taken together, our 3D structural models of nSH3 and cSH3 domains in complex with Sos1 peptide shed new light on their binding specificity and structure–activity relationships. Unlike several previous studies [21–24], in which various acidic residues have

been suggested to participate in stabilizing the positive charge on the R_{+5} residue in the consensus motif PPVPPR, our thermodynamic data demonstrate here that this role is exclusively fulfilled by D15 in the nSH3 domain and E171 in the cSH3 domain. Our structural data further argue that the spatial positioning of D15 and E171 in the β-barrel fold is consistent with their role in defining the differential binding of nSH3 and cSH3 domains to Sos1.

Conclusions

Discovered over two decades ago as a non-catalytic component of various adaptors and enzymes [43], the SH3 domain is believed to be the most ubiquitous protein module amongst the vast arsenal employed by signaling machinery in mammalian cells. This notion is further supported by the fact that the human genome encodes for over 300 homologues of SH3 domains across a diverse plethora of proteins involved in a wide variety of activities from cell growth and proliferation through cell cycle regulation and developmental control to apoptosis and cancer. It then hardly comes as a surprise that Pubmed search of SH3 domain delivers nearly 5000 hits, more than for any other protein module, underlying extensive studies that have been carried out to explore the biological function and diversity of this important component of cellular signaling. Despite such wealth of knowledge, our understanding of the SH3-ligand specificity remains hitherto severely limited. Various attempts over the past decade to design computer algorithms to predict the specificity of SH3 domains against potential ligands have not only eluded theoreticians but also point to the need for further experiment.

In this study, we were driven by the curiosity to unravel the underlying structural basis for the differential binding of SH3 domains of Grb2 to Sos1 – a classical SH3–ligand interaction that has not only been widely studied but its role in determining the fate of a healthy from a diseased cell cannot be disputed. It was thus fitting that we chose this key protein–protein interaction to further expand our knowledge of SH3-ligand specificity. Our data are consistent with the hypothesis that the residue D15 in the RT loop within the nSH3 domain is the major determinant of high affinity binding to Sos1 relative to the cSH3 domain by virtue of its ability to engage in the formation a salt bridge with R_{+5} residue in the consensus motif PPVPPR. In contrast, the residue analogous to D15 in the cSH3 domain is G173. Thus, the lack of a chemically and structurally equivalent residue at this key position in the RT loop of the β-barrel fold of cSH3 domain accounts for its low affinity binding to Sos1. That this is even possible is resurrected by the presence of a neighboring E171 in the cSH3 domain that appears to substitute for the role of D15 in the nSH3 domain. The differential binding affinities and differential thermodynamic mechanisms employed by the SH3 domains of Grb2 in their ability to recognize Sos1 may have evolved to provide a molecular switch necessary to regulate the interactions of Grb2 with a diverse array of downstream effectors of Grb2 in addition to Sos1 depending on the biological context and the nature of mitogenic stimuli [3,10–17].

It should be noted here that SH3 domains are generally believed to interact with their cognate ligands with an affinity in the 1–10 μM range. However, this school of thought is largely based on studies carried out in buffers that show significant deviations from situations that are likely to be encountered within the complex milieu of the living cell. In particular, an increasing number of the SH3–ligand binding studies have been carried out in buffers that have tended to be devoid of salt. Our study here shows that salt tightly modulates the Grb2–Sos1 interaction and that this is likely to be the rule rather than an exception for the SH3–ligand interaction in general due to the universal requirement of one or more salt bridges that play a critical role in defining specificity between this pair of protein–protein interactions [25,44–46]. Assuming that an aqueous solution with ionic strength of around 200 mM is a bona fide mimic of the physiological milieu of the living cell, our data presented here show that SH3 domains are more likely to bind to their cognate ligands with an affinity in the 10–100 μM range in lieu of 1–10 μM. What we have not argued thus far is the realization that a vast number of SH3-proteins contain SH3 domains in multiple copies and often in tandem. Complementing this exquisite multiple-domain architecture is the design of SH3 ligands which also tend to boast multiple proline-rich motifs within the same stretch of a polypeptide chain, with Sos1 being a classical example of this class of polydentate SH3 ligands. Thus, it seems likely that the simultaneous binding of multiple SH3 domains to multiple ligand sites may result in pronounced binding affinities, due to entropic advantage, instead of those inferred from the analysis of isolated SH3 domains with their cognate ligands. Sos1 indeed contains multiple proline-rich sequences containing the consensus motif PPVPPR. It is thus conceivable that the SH3 domains of Grb2 bind to Sos1 simultaneously and thereby leading to enhancement of Grb2–Sos1 interaction.

In short, our data reported here provide key insights into the structural basis of the differential binding of SH3 domains of Grb2 to Sos1 and significantly contribute to our understanding of the molecular determinants of SH3–ligand specificity. Because of our poor understanding of the biophysical principles that underlie this specificity, our attempts to design novel inhibitors to disrupt this key protein–protein interaction pertinent to cellular signaling and cancer have meet little success to date. Further biophysical analysis of SH3–ligand interactions is thus clearly warranted to expand our knowledge of the biology of SH3 domains and to help pave the way for the design of novel and more effective anti-SH3 inhibitors.

Acknowledgments

This work was supported by funds from the UM/Sylvester Braman Family Breast Cancer Institute and the American Heart Association grant (#0655087B) to AF. We thank Cédric Georges of Bio-Logic for help with CD data collection.

References

[1] P. Chardin, D. Cussac, S. Maignan, A. Ducruix, FEBS Lett. 369 (1995) 47–51.
[2] A. Nimnual, D. Bar-Sagi, Sci. STKE 2002 (2002) PE36.
[3] N. Li, A. Batzer, R. Daly, V. Yajnik, E. Skolnik, P. Chardin, D. Bar-Sagi, B. Margolis, J. Schlessinger, Nature 363 (1993) 85–88.
[4] N.W. Gale, S. Kaplan, E.J. Lowenstein, J. Schlessinger, D. Bar-Sagi, Nature 363 (1993) 88–92.
[5] A.M. Cheng, T.M. Saxton, R. Sakai, S. Kulkarni, G. Mbamalu, W. Vogel, C.G. Tortorice, R.D. Cardiff, J.C. Cross, W.J. Muller, T. Pawson, Cell 95 (1998) 793–803.
[6] M. Rozakis-Adcock, J. McGlade, G. Mbamalu, G. Pelicci, R. Daly, W. Li, A. Batzer, S. Thoma, J. Brugge, P.G. Pelicci, J. Schlessinger, T. Pawson, Nature 360 (1992) 689–692.
[7] E.J. Lowenstein, R.J. Daly, A.G. Batzer, W. Li, B. Margolis, R. Lammers, A. Ullrich, E.Y. Skolnik, D. Bar-Sagi, J. Schlessinger, Cell 70 (1992) 431–442.
[8] M. Rozakis-Adcock, J. McGlade, G. Mbamalu, G. Pelicci, R. Daly, W. Li, A. Batzer, S. Thomas, J. Brugge, P.G. Pelicci, et al., Nature 360 (1992) 689–692.
[9] M. Rozakis-Adcock, R. Fernley, J. Wade, T. Pawson, D. Bowtell, Nature 363 (1993) 83–85.
[10] P. Chardin, J.H. Camonis, N.W. Gale, L. van Aelst, J. Schlessinger, M.H. Wigler, D. Bar-Sagi, Science 260 (1993) 1338–1343.
[11] U. Schaeper, N.H. Gehring, K.P. Fuchs, M. Sachs, B. Kempkes, W. Birchmeier, J. Cell. Biol. 149 (2000) 1419–1432.
[12] M. Lewitzky, C. Kardinal, N.H. Gehring, E.K. Schmidt, B. Konkol, M. Eulitz, W. Birchmeier, U. Schaeper, S.M. Feller, Oncogene 20 (2001) 1052–1062.
[13] K. Seedorf, G. Kostka, R. Lammers, P. Bashkin, R. Daly, W.H. Burgess, A.M. van der Bliek, J. Schlessinger, A. Ullrich, J. Biol. Chem. 269 (1994) 16009–16014.
[14] M. Vidal, J.L. Montiel, D. Cussac, F. Cornille, M. Duchesne, F. Parker, B. Tocque, B.P. Roques, C. Garbay, J. Biol. Chem. 273 (1998) 5343–5348.
[15] H. Odai, K. Sasaki, A. Iwamatsu, Y. Hanazono, T. Tanaka, K. Mitani, Y. Yazaki, H. Hirai, J. Biol. Chem. 270 (1995) 10800–10805.
[16] R.K. Park, W.T. Kyono, Y. Liu, D.L. Durden, J. Immunol. 160 (1998) 5018–5027.

[17] S.J. Moeller, E.D. Head, R.J. Sheaff, Mol. Cell. Biol. 23 (2003) 3735–3752.
[18] G.W. Reuther, C.J. Der, Curr. Opin. Cell Biol. 12 (2000) 157–165.
[19] M.J. Robinson, M.H. Cobb, Curr. Opin. Cell Biol. 9 (1997) 180–186.
[20] D. Kohda, H. Terasawa, S. Ichikawa, K. Ogura, H. Hatanaka, V. Mandiyan, A. Ullrich, J. Schlessinger, F. Inagaki, Structure 2 (1994) 1029–1040.
[21] M. Wittekind, C. Mapelli, B.T. Farmer 2nd., K.L. Suen, V. Goldfarb, J. Tsao, T. Lavoie, M. Barbacid, C.A. Meyers, L. Mueller, Biochemistry 33 (1994) 13531–13539.
[22] M. Wittekind, C. Mapelli, V. Lee, V. Goldfarb, M.S. Friedrichs, C.A. Meyers, L. Mueller, J. Mol. Biol. 267 (1997) 933–952.
[23] N. Goudreau, F. Cornille, M. Duchesne, F. Parker, B. Tocque, C. Garbay, B.P. Roques, Nat. Struct. Biol. 1 (1994) 898–907.
[24] H. Terasawa, D. Kohda, H. Hatanaka, S. Tsuchiya, K. Ogura, K. Nagata, S. Ishii, V. Mandiyan, A. Ullrich, J. Schlessinger, et al., Nat. Struct. Biol. 1 (1994) 891–897.
[25] H. Yu, J.K. Chen, S. Feng, D.C. Dalgarno, A.W. Brauer, S.L. Schreiber, Cell 76 (1994) 933–945.
[26] J.Y. Kato, T. Takeya, C. Grandori, H. Iba, J.B. Levy, H. Hanafusa, Mol. Cell. Biol. 6 (1986) 4155–4160.
[27] E. Gasteiger, C. Hoogland, A. Gattiker, S. Duvaud, M.R. Wilkins, R.D. Appel, A. Bairoch, Protein identification and analysis tools on the ExPASy server, in: J.M. Walker (Ed.), The Proteomics Protocols Handbook, Humana Press, Totowa, New Jersey, USA, 2005, pp. 571–607.
[28] T. Wiseman, S. Williston, J.F. Brandts, L.N. Lin, Anal. Biochem. 179 (1989) 131–137.
[29] J.B. Chaires, Anticancer Drug Des. 11 (1996) 569–580.
[30] M.T. Record Jr., M.L. Lohman, P. De Haseth, J. Mol. Biol. 107 (1976) 145–158.
[31] J. Wyman Jr., Adv. Protein Chem. 19 (1964) 223–286.
[32] T.M. Lohman, D.P. Mascotti, Methods Enzymol. 212 (1992) 400–424.
[33] M.A. Marti-Renom, A.C. Stuart, A. Fiser, R. Sanchez, F. Melo, A. Sali, Annu. Rev. Biophys. Biomol. Struct. 29 (2000) 291–325.
[34] M. Carson, J. Appl. Crystallogr. 24 (1991) 958–961.
[35] R. Koradi, M. Billeter, K. Wuthrich, J. Mol. Graph 14 (1996) 51–55.
[36] X. Siebert, L.M. Amzel, Proteins 54 (2004) 104–115.
[37] K.P. Murphy, D. Xie, K.S. Thompson, L.M. Amzel, E. Freire, Proteins 18 (1994) 63–67.
[38] A. Tamura, P.L. Privalov, J. Mol. Biol. 273 (1997) 1048–1060.
[39] K.P. Murphy, Med. Res. Rev. 19 (1999) 333–339.
[40] E. Freire, Arch. Biochem. Biophys. 303 (1993) 181–184.
[41] B.M. Baker, K.P. Murphy, Methods Enzymol. 295 (1998) 294–315.
[42] K.H. Lee, D. Xie, E. Freire, L.M. Amzel, Proteins 20 (1994) 68–84.
[43] B.J. Mayer, M. Hamaguchi, H. Hanafusa, Nature 332 (1988) 272–275.
[44] W.A. Lim, F.M. Richards, R.O. Fox, Nature 372 (1994) 375–379.
[45] A.B. Sparks, J.E. Rider, N.G. Hoffman, D.M. Fowlkes, L.A. Quillam, B.K. Kay, Proc. Natl. Acad. Sci. U.S.A. 93 (1996) 1540–1544.
[46] G. Cesareni, S. Panni, G. Nardelli, L. Castagnoli, FEBS Lett. 513 (2002) 38–44.